

Article

Self-Cleaning and Antibacterial Properties of the Cement Mortar with ZnO/Hydroxyapatite Powders

Ana-Maria Mocioiu ^{1,*}, Ileana Mohanu ², Roxana Mioara Piticescu ¹ , Ioan Albert Tudor ¹ , Ionela Petre ², Mihai Ghiță ¹, Andreea Nicoleta Ghiță ¹, Miruna Adriana Ioța ¹, Nicoleta Vitan ^{1,*}, Mădălin Enache ³  and Simona Neagu ³ 

¹ National Research & Development Institute for Non-Ferrous and Rare Metals—IMNR, Biruinței Blvd. 102, Ilfov, 077145 Pantelimon, Romania

² CEPROCIM S.A., Preciziei Blvd, District 6, 062203 Bucharest, Romania

³ Institute of Biology Bucharest of Romanian Academy—IBB, 296 Splaiul Independentei, P.O. Box 56-53, 060031 Bucharest, Romania

* Correspondence: ammocioiu@imnr.ro (A.-M.M.); nvitan@imnr.ro (N.V.)

Abstract: According to literature data, different micro- and nanopowders have been used as a partial substitute for cement mortar due to their small size and large specific surface area. The aim of the work is to develop innovative materials based on cement mortar with antibacterial and self-cleaning properties, which can be used in the long-term maintenance of clean spaces. First, zinc oxide/hydroxyapatite (ZnO/Hap) powder denoted as ZH was synthesized by the hydrothermal method; then it was characterized by X-ray diffraction (XRD), scanning electron microscopy (SEM)/energy dispersive spectroscopy (EDS), and adsorption–desorption isotherms. The second step was the cement mortar preparation: one plain, denoted E, and one with ZH powder inside, denoted MZH. Both mortars were subjected to self-cleaning and antibacterial tests. In the self-cleaning tests, two concentrated solutions of rhodamine B and methylene blue were used. MZH showed a better decolorating after 24 h of UV light than plain cement mortar denoted E for both solutions. In order to highlight the antibacterial effect of cement mortars on some strains of Gram-positive and Gram-negative bacteria, the direct contact method was used. The study revealed that, after 24 h of incubation, the planktonic growth of the *E. coli* strain is significantly inhibited in the presence of the MZH sample, compared to the control strain. MZH cement mortar exhibits a better growth inhibitory property than the plain cement mortar E.

Keywords: cement mortar; ZnO/Hap; hydrothermal; self-cleaning; antibacterial properties



Citation: Mocioiu, A.-M.; Mohanu, I.; Piticescu, R.M.; Tudor, I.A.; Petre, I.; Ghiță, M.; Ghiță, A.N.; Ioța, M.A.; Vitan, N.; Enache, M.; et al. Self-Cleaning and Antibacterial Properties of the Cement Mortar with ZnO/Hydroxyapatite Powders. *Inorganics* **2022**, *10*, 241. <https://doi.org/10.3390/inorganics10120241>

Academic Editor: Kenneth J.D. MacKenzie

Received: 19 October 2022

Accepted: 28 November 2022

Published: 5 December 2022

Publisher's Note: MDPI stays neutral with regard to jurisdictional claims in published maps and institutional affiliations.



Copyright: © 2022 by the authors. Licensee MDPI, Basel, Switzerland. This article is an open access article distributed under the terms and conditions of the Creative Commons Attribution (CC BY) license (<https://creativecommons.org/licenses/by/4.0/>).

1. Introduction

An innovative approach for the concrete sector to solve the prevailing problems in the construction industry is the addition of oxide nano- and microparticles. According to literature data, different particles have been used as a partial substitute for cement due to their small size and large specific surface area.

Construction materials such as cements modified with particles are intensively studied today for improving air purification and pollutant degradation properties [1–20].

Currently, titanium dioxide (TiO₂) is the most widely used applied photocatalyst, due to its self-cleaning functions, air purification capacity, and antibacterial capacity [1–4]. However, titanium dioxide nanoparticles easily agglomerate in cement mortar due to the high surface energy, therefore, a process for separating the particles from the agglomerates (e.g., ultrasonic dispersion) is necessary. In practice, it is difficult to achieve a uniform dispersion of the particles due to their strong cohesion. So, micrometer particles can have a better action.

The beneficial role of zinc oxide nanoparticles in improving cement performance has been previously studied [9]. Nanoparticles of zinc oxide (ZnO) have a unique antimicrobial

and photocatalytic activity. They have a filling effect and have been shown to influence the hydration reaction in cement. It has been found that the introduction of ZnO nanoparticles improves the photocatalytic properties of cement. The impact of ZnO nanoparticles on microstructure and resistance was discussed. The study shows that mortars with an optimized quantity of nanoparticles may have increased mechanical strength and antimicrobial properties.

Another way to obtain better cements is the introduction into the composition of SiO₂ (SP) and ZnO mesoscopic powder (ZP), obtained by a sol–gel method. Commercial SP and ZP were mixed in different quantities with Portland cements, and their influence on the hydration–hardening processes and antibacterial properties of the resulting cement was evaluated [10]. The compression resistances of nano-SiO₂ particle mortars were all higher than those of silica fume-containing mortars at 7 and 28 days [11]. Jo [11] demonstrated that silica fume nanoparticles are more valuable in increasing resistance. The modification of the cement with nan-silica has been studied to improve compressive strength and resistance to environmental factors [12–14]. The effect of introducing silica nanoparticles into the cement binder is to accelerate hydration by introducing additional active places to increase the C-S-H phase, and increase the resistance during the initial period of densification of the microstructure [12].

Antibacterial results against *E. coli* strains were obtained by Dehkordi et al. [18] on cement pastes containing ZnO nanoparticles during hydration. However, the samples were small (3 mm) and the cements were not allowed to harden like the walls of clean places. So, the results on real walls may be different. The authors also used polyethylene glycol (PEG), an addition that is not usually used in the composition of cement.

In nature, hydroxyapatite (Hap) is found in rocks and in the hard tissues of human and animal bodies. Hydroxyapatite (Hap) is a naturally occurring mineral form of calcium apatite with the formula Ca₅(PO₄)₃(OH). The crystal unit cell comprises two entities (one of phosphate and one of hydroxide) as can be seen in the enlarged formula Ca₁₀(PO₄)₆(OH)₂. It crystallizes in the hexagonal crystal system. Pure hydroxyapatite powder has a white color. Another approach is the use of hydroxyapatite (Hap), Ca₅(PO₄)₃(OH), mixed with an antibacterial agent such as ZnO. Hap is a natural constituent of many Earth rocks [21], and it makes up the mineral constituent of hard tissues (teeth, bones) in vertebrates [22–24], hence its biocompatible feature that leads to several applications in biomedical sciences [21,25]. Hap usually crystallizes in the hexagonal space group P6₃/m [21]. The current state of the art is to synthesize hydroxyapatite with nanometric dimensions with properties similar to the natural one. Hydroxyapatite is a good material for implants as well as for other applications, due to its non-toxic effects, corrosion resistance, and high mechanical strength.

The aim of the work is to develop innovative materials based on cement mortar and zinc oxide/hydroxyapatite powders (ZH), with antibacterial and self-cleaning properties, which can be used in the long-term maintenance of clean spaces.

2. Materials and Methods

The zinc oxide/hydroxyapatite powder was obtained by the hydrothermal process, in a single step, using as raw materials Zn(NO₃)₂·6H₂O, Ca(NO₃)₂·4H₂O, (NH₄)H₂PO₄, which were dissolved in distilled water and precipitated with ammonia solution (NH₃ 25%). The molar compositions of the raw materials Zn(NO₃)₂·6H₂O, Ca(NO₃)₂·4H₂O, (NH₄)H₂PO₄ are 1:1.1:1.66. The mixture was introduced into the hydrothermal synthesis autoclave, and the parameters were set as: temperature 200–230 °C and pressure between 90 and 120 atm for 2 h. After the hydrothermal synthesis, the solutions were filtered, and the obtained precipitate was washed until the pH was neutral, and dried in an oven. Hydrothermal synthesis was carried out in a stainless steel BERGHOF autoclave, Germany, with a volume of 5.5 L, 300 °C maximum work temperature, 150 atm maximum pressure, with PID controller, computerized recording of parameters, sample collection during the process, and controlled cooling. The powders were dried in a programmable Memmert TWW-UFE 400 oven, maximum temperature 250 °C. The synthesis was repeated four times.

The obtained powders were also characterized from a morphological and structural point of view.

For the structural characterization, a Bruker-AXS D8 ADVANCE Bragg–Brentano diffractometer with radiation source (Cu) and SOL X detector in vertical θ – θ geometry, provided with BRUKER AXS software, was used. Diffraction spectra were acquired in the angular range 6–70°, in continuous mode, with a step of 0.02°. Phase identification was carried out with the DIFFRAC.EVA release 2022 program and the ICDD PDF 4 + 2022 database.

The study of powder morphology was carried out with a Quanta 250 scanning electron microscope, in high vacuum (HV) mode, using a secondary electron detector (ETD), electron backscattered detector (CBS), and energy dispersive spectroscopy (EDS) detector.

The surface area and N₂ adsorption/desorption characteristics were established with a BET apparatus.

The cement mortar whose mechanical characteristics fall into one of the plaster mortars classes CS I–CS IV, according to SR EN 998-1 (Specification of mortars for masonry. Part 1: Mortar for plastering and smoothing), was etalon [26]. The cement was of CEM I type, obtained by simultaneously grinding clinker with 3% set retarder (gypsum), to a fineness expressed as Blaine specific surface area of approx. 3500 cm²/g. Two samples of cement mortar: one plain cement mortar denoted E and one cement mortar with the addition of zinc oxide/hydroxyapatite particles denoted MZH, were made. Both compositions contain the same proportions: sand, cement, and limestone filler, and they have controlled properties [26,27]. The cement mortars with dimensions 5 × 5 × 5 cm were aged 28 days.

Self-cleaning tests were performed by spraying rhodamine B and methylene blue on 5 × 5 × 5 cm samples of cement mortars. The cement mortars were separated into two groups. The cement mortars from the first group were stained by spraying with a solution of rhodamine B with a high concentration of 2 g/L, and those from the second group were stained by spraying with a solution of methylene blue with a high concentration of 2.5 g/L. All samples were half covered with a strip of white paper through which UV radiation did not pass. The ULTRA VITALUX 300 W lamp was used for the tests, with the following characteristics: lamp current 1.3 A, nominal power 300.00 W, photometric data: the radiation power in the wavelength range 315...400 nm (UVA) is 13.6 W, the radiation power in the range of wavelengths 280...315 nm (UVB) is 3.0 W. All contaminated cement mortars were placed under the UV lamp in a closed enclosure where no outside light penetrated for 24 h.

In order to confirm the self-cleaning properties of the mortar cement MZH, colorimetric measurements by a Datacolor 650TM Series dual-beam spectrophotometer equipped with Datacolor Tools plus V2 software were performed.

The equipment used to measure ultra-precise reflectance has the following characteristics: measurement geometry: diffuse illumination and 8° viewing; illumination source: pulsed xenon filtered to approximate D65; sphere diameter: 152 mm/6.0 in; specular port: automated included or excluded; wavelength range: 360 nm to 700 nm; aperture plates for reflection measurements: SAV-9 mm illuminated, 5 mm measured; transmission sampling aperture size: 22 mm.

Assessment of color is more than a numeric expression. Usually, it is an assessment of the color difference (ΔE) from a known standard. CIELAB (L*a*b*) and CIELAB (L*C*h) are used to compare the colors of two objects. The CIELAB color space, referred to as L*a*b*, is a color space defined by the International Commission on Illumination (abbreviated CIE) in 1976.

The CIELAB space is three-dimensional and covers the entire gamut (range) of human color perception. It is based on the opponent color model of human vision, where red and green form an opponent pair and blue and yellow form an opponent pair. The lightness value, L*, also referred to as "Lstar," defines black at 0 and white at 100. The a* axis is relative to the green–red opponent colors, with negative values toward green and positive values toward red. The b* axis represents the blue–yellow opponents, with negative numbers

toward blue and positive toward yellow. The expressions for these color differences are DL^* , Da^* , Db^* , or $DL^* DC^* DH^*$ ("D" symbolizes "delta," which indicates difference).

The parameters measured with the Datacolor equipment are defined below according to the standards of the Commission Internationale de l'Éclairage (the International Commission on Illumination): DL^* = difference in lightness/darkness value (+ = lighter – = darker); Da^* = difference on red/green axis (+ = redder – = greener); Db^* = difference on yellow/blue axis (+ = yellower – = bluer); DC^* = difference in chroma (+ = brighter – = duller); DH^* = difference in hue; DE^* = total color difference value.

The equipment software uses formulas defined by Kubelka and Munk for calculating the optical properties of the absorption and scattering coefficients.

In order to highlight the antibacterial effect of cement mortars on some strains of Gram-positive and Gram-negative bacteria, the direct contact method was used. The cement mortars were cut to sizes of $1.5 \times 1.5 \times 0.5$ cm (L \times W \times H), and sterilized for 60 min using a UV lamp prior to testing. In this study, the following reference strains from the American Type Culture Collection (ATCC) were used: *Salmonella enterica* subsp. *enterica* serovar *Typhimurium* ATCC 14028 (*S. enterica*), *Staphylococcus aureus* ATCC 25923 (*S. aureus*), *Pseudomonas aeruginosa* ATCC 15442 (*P. aeruginosa*), and *Escherichia coli* ATCC 25922 (*E. coli*). The growth medium for the bacterial strains was tryptic soy broth (TSB, Scharlab, Barcelona, Spain). A sterile saline suspension obtained from an 18 h old young culture with a cell density of 1.5×10^8 CFU/mL (0.5 McFarland), spectrophotometrically adjusted by measuring the absorbance at a wavelength of 660 nm ($A_{660} = 0.08$), constituted the standardized inoculum. Evaluation of sample efficiency was performed in sterile 24-well Greiner microplates. A piece of mortar was placed in each well, over which 1 mL of culture medium and 10 μ L of standardized bacterial suspension were added. The prepared plates were incubated at 37 °C for 24 h, under static conditions. At the end of the incubation period, 200 μ L of the resultant microbial culture was transferred to sterile 96-well Greiner microplates, and the turbidity (absorbance, Abs 600 nm) was determined spectrophotometrically. Experiments were performed in duplicate.

3. Results

3.1. Zinc Oxide/Hydroxyapatite Powder (ZH)

3.1.1. X-ray Diffraction (XRD) of ZH Powder

Figure 1 presents the XRD pattern of the ZH powder and identification of crystalline phases. Two phases were identified: zincite, ZnO, (card no. 04-015-4060), with hexagonal crystallization, and hydroxyapatite, $Ca_5(PO_4)_3(OH)$ (card no. 01-079-5683), in a hexagonal crystallization system too. XRD analysis shows a well-defined peak at $2\theta = 31.80^\circ$ which is characteristic of (211) atomic plane diffraction of hydroxyl apatite. The peaks at 2θ of 36.5° , 56.8° , 34.59° are characteristic to ZnO crystals with preferential growth direction c. The well-defined peak at 36.5 is characteristic of (101) atomic plane diffraction of ZnO. In addition, the high intensity of the diffraction lines suggests the highly crystalline nature of the prepared powder.

3.1.2. Scanning Electron Microscopy (SEM) of ZH Powder

The morphology of the ZH powder was investigated with scanning electron microscopy (SEM), and the composition of the particles was evaluated by dispersive energy spectroscopy (EDS). The ZH powder was coated with a thin layer of gold for better conductivity. Figure 2a shows the SEM image of the powder and two types of crystals can be observed. Compositional identification of the two types of crystals was carried out using EDS, and the results are shown in Figure 2b,c and in Table 1. Some crystals were formed into rods with diameters about 3–4 μ m and length of 10–20 μ m. Other crystals show a cuboidal grain. The composition of the rods (point 1) is formed mainly in the elements Zn and O, and the composition of the grains consists predominantly of elements of hydroxyapatite (Ca, P, O). As can be seen from Figure 2 and Table 1, both types of crystals have zinc and calcium in their composition. There are two phases as can be seen in the

XRD pattern: one rich in ZnO and one rich in hydroxyapatite. An optimum Ca/P ratio (1.79 at%) was recorded for hydroxyapatite crystals.

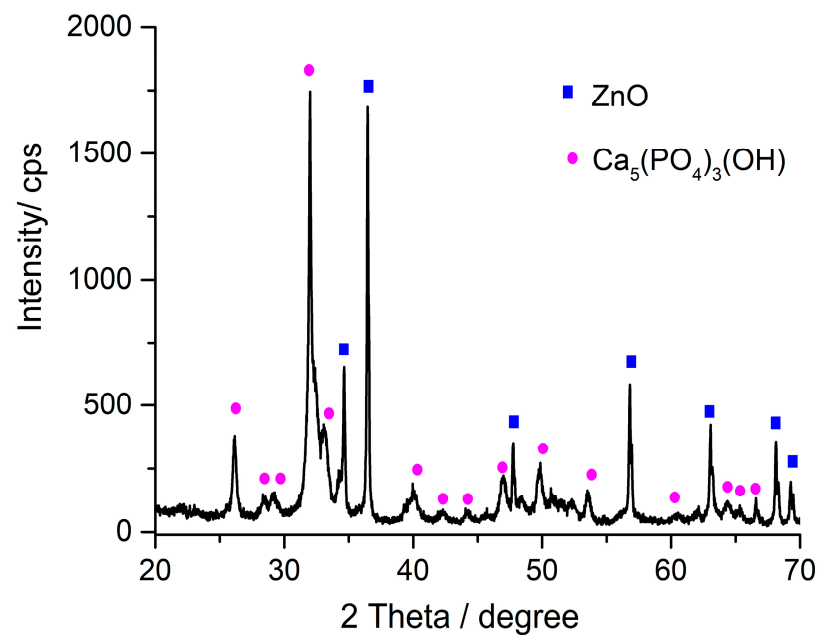
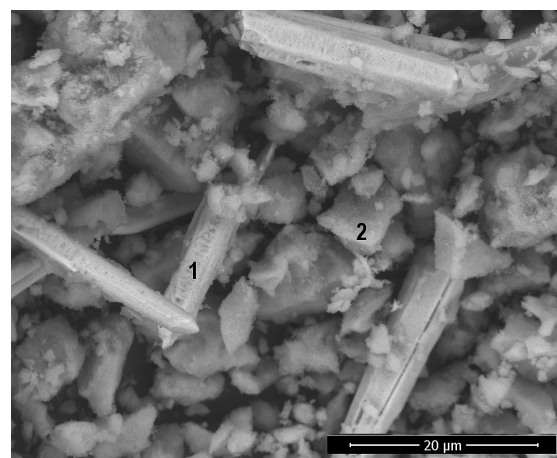
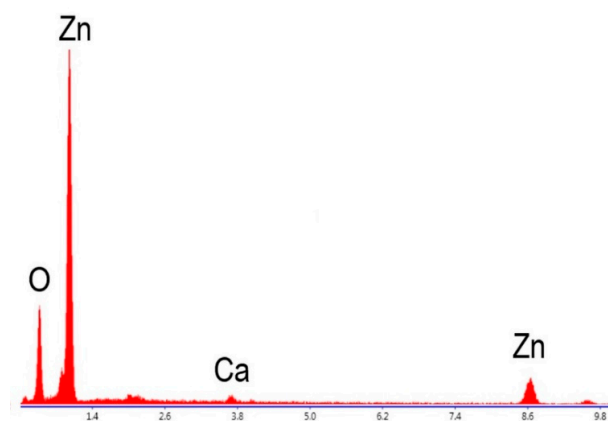


Figure 1. XRD pattern of the ZH powder.



(a)



(b)

Figure 2. Cont.

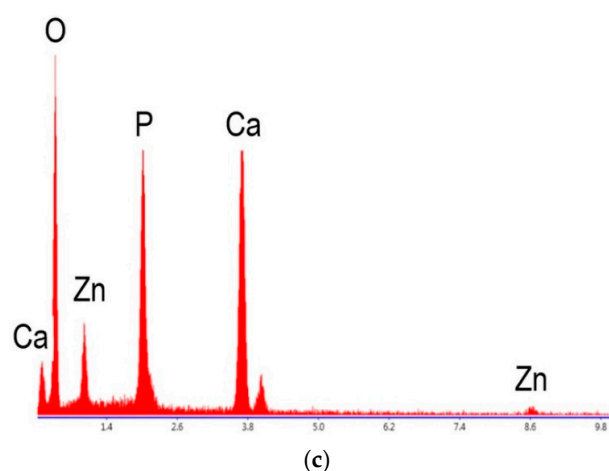


Figure 2. SEM/EDS images of the ZH powder: (a) SEM image of the powder; (b) EDS analysis of point 1; EDS analysis of point 2.

Table 1. Chemical composition of the ZH powder determined by energy dispersive spectroscopy.

| Point 1 | | | | Point 2 | | | |
|---------|----------|----------|---------|---------|----------|----------|---------|
| Element | Weight % | Atomic % | Error % | Element | Weight % | Atomic % | Error % |
| O | 18.94 | 48.39 | 9.44 | O | 38.13 | 59.76 | 11.53 |
| Ca | 2.38 | 2.42 | 19.37 | P | 16.72 | 13.54 | 4.63 |
| Zn | 78.68 | 49.19 | 6.81 | Ca | 38.76 | 24.25 | 3.54 |
| | | | | Zn | 6.39 | 2.45 | 34.03 |

3.1.3. Adsorption–Desorption Isotherms of ZH Particles

The powder was analyzed in a nitrogen atmosphere (adsorption–desorption isotherms at 77 K). Figure 3 shows adsorption–desorption isotherms of the ZH powder. The moisture content of the powder was removed by drying it at 300 °C for 3 h before the analysis. The adsorption volumes of particles increase as P/P0 increases. BET surface area is 86.70 m²/g and pore volume is 0.0544 cm³/g. The adsorption and desorption curves have the same shape due to uniform pore structure.

3.2. Cement Mortar Acquisition and Characterization

Two samples of cement mortar, a simple cement mortar denoted E and a cement mortar with the addition of powder ZH denoted MZH, were studied to determine which of them has the best properties. Both cement mortars contain the same proportions of sand, cement, and limestone filler in accordance with patent SR EN 998-1:2016 [26] and they have properties according to SR EN 1015-11:2020 [27].

3.2.1. Self-Cleaning Properties

Self-cleaning tests were performed by spraying rhodamine B and methylene blue on 5 × 5 × 5 cm samples of cement mortars. All colored cement mortars with and without ZH powders were placed under the UV lamp in a closed enclosure where no outside light penetrated for 24 h. The figures below show the samples before and after exposure to UV light. In Figure 4 are the cement mortars after self-cleaning tests, where some samples were covered and others were exposed to UV light. The decoloring of the cement mortars is correlated with self-cleaning properties. As can be seen in the figure, the cement mortar MZH with ZH powder has better self-cleaning properties than plain cement mortar.

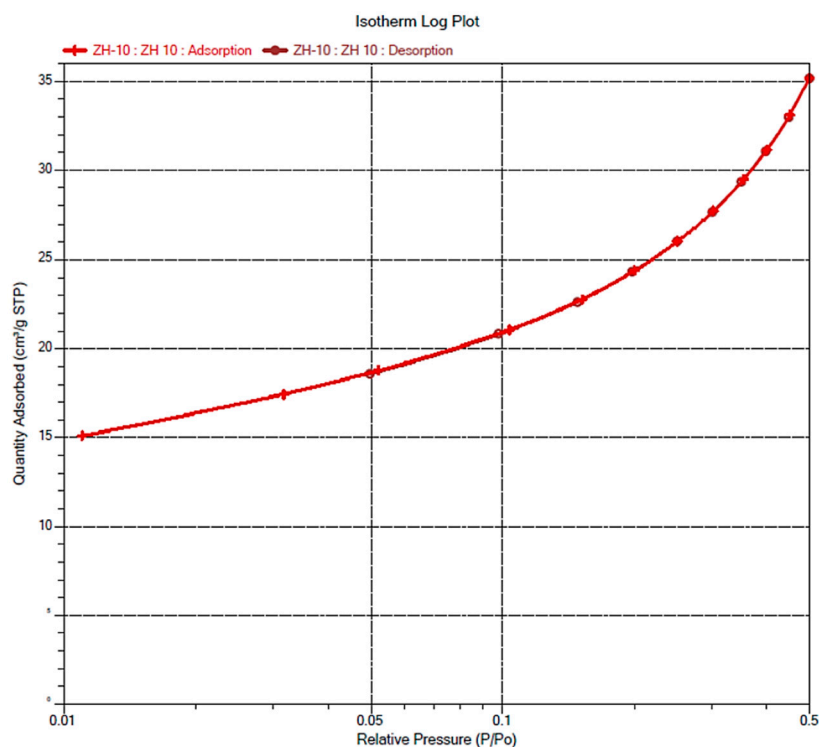


Figure 3. N₂ adsorption/desorption curves obtained by BET.

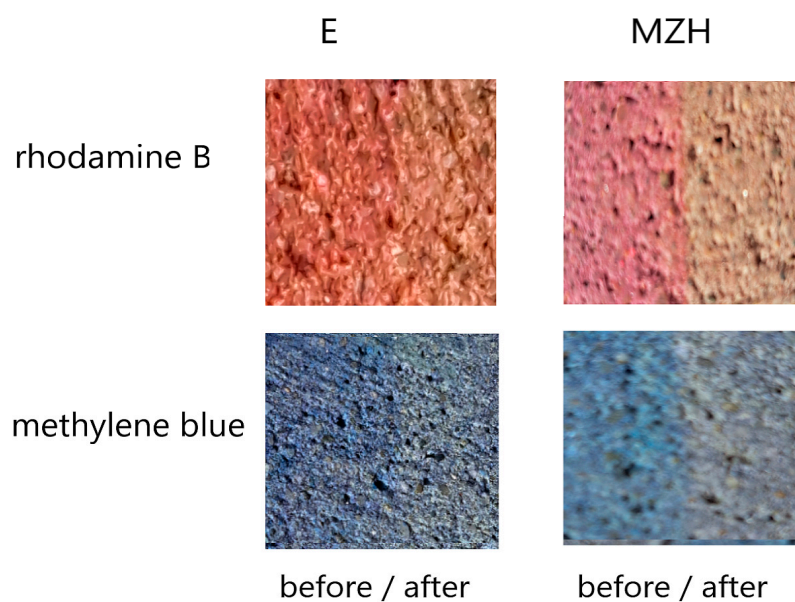


Figure 4. Images of self-cleaning result for plain cement mortar (E) and cement mortar with powder ZnO/Hap (MZH).

The color difference was measured in the MZH mortar cement presented in Figure 4, in three points in the UV exposed zone named bright areas 1, 2, 3 and another three points in the unexposed zone named dark areas 1, 2, 3. An unstained cement mortar was used as a standard.

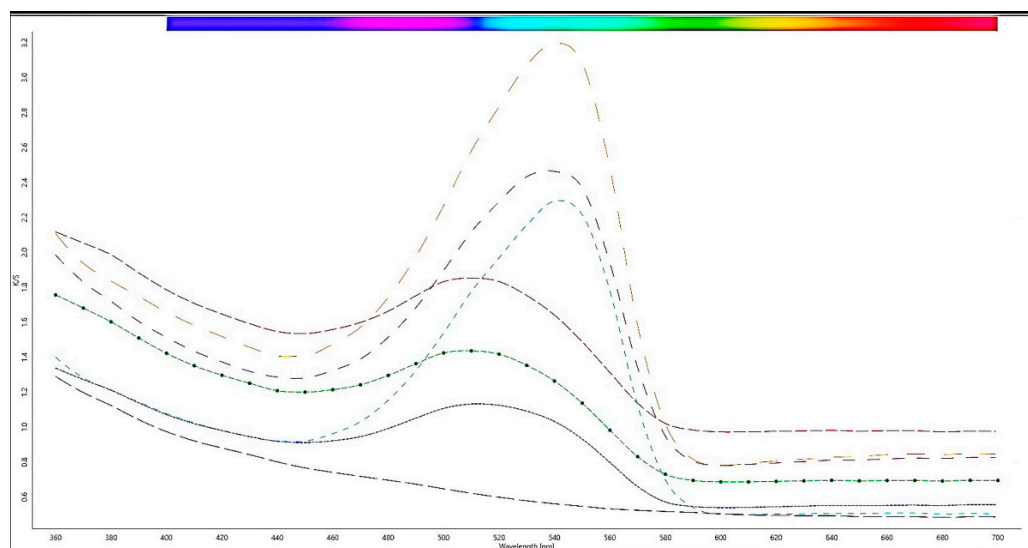
As can be seen from the data presented in Table 2, the values of the color difference CIE DL are lower in the points on the surface exposed to UV than in the points on the non-exposed surface, confirming the high degree of discoloration. At the same time, the CIE Da values confirm that the darker area is closer to the red color, while the lighter area is closer to the gray color of the initial standard.

Table 2. CIELAB coefficients of MZH mortar cement.

| Batch Name | CIE DL* | CIE Da* | CIE Db* | CIE DC* | CIE DH* | CIE DE* |
|---------------|---------|---------|---------|---------|---------|---------|
| Standard | −0.01 | 0.00 | 0.00 | 0.00 | 0.00 | 0.01 |
| Bright area 1 | −6.58 | 8.47 | −2.15 | 3.28 | −8.10 | 10.94 |
| Bright area 2 | −3.90 | 8.90 | −1.28 | 4.06 | −8.02 | 9.80 |
| Bright area 3 | −3.98 | 8.89 | −1.04 | 4.18 | −7.92 | 9.80 |
| Dark area 1 | −10.36 | 18.97 | −8.72 | 12.85 | −16.45 | 23.31 |
| Dark area 2 | −13.24 | 17.74 | −8.84 | 11.65 | −16.04 | 23.84 |
| Dark area 3 | −12.78 | 17.02 | −7.45 | 10.80 | −15.11 | 22.55 |

The parameters measured with the Datacolor equipment are defined below according to the CIE standards for Commission Internationale de l'Éclairage (the International Commission on Illumination): DL* = difference in lightness/darkness value (+ = lighter − = darker); Da* = difference on red/green axis (+ = redder − = greener); Db* = difference on yellow/blue axis (+ = yellower − = bluer); DC* = difference in chroma (+ = brighter − = duller). DH* = difference in hue; DE* = total color difference value.

Figure 5 shows the spectra in the visible region for all measured areas, as in Table 2. The higher intensity of the dark areas and the lower intensity of the areas after photocatalysis are shown. In Figure 5, the x -axis represents the wavelengths in nm in the UV–Vis range, and the y -axis represents K/S. K represents the absorption coefficient and S is scattering coefficient, the value K/S is a measurement of surface color strength. The curve at the bottom of the plot without a band is the initial unstained MZH cement mortar (denoted as standard in Table 2). In the other spectra, the bands at around 550 nm are characteristic of the dye rhodamine B. The three measurements on the colored area (denoted as the dark area in Table 2) and three measurements on the UV exposed (photocatalysis) colored area (denoted as the bright area in Table 2) were performed. This is also confirmed by the wavelength shift from approximately 520 nm in the bright area (toward green) to approximately 555 nm in the dark area (toward red). The results confirm the self-cleaning properties.

**Figure 5.** Representation of the measurement of surface color strength (K/S) versus wavelength in UV–Vis for MZH cement mortar.

3.2.2. Antibacterial Properties

The results of planktonic growth demonstrated that the cement mortars showed different antimicrobial effects, depending on their composition. Figure 6 shows the sensitivity of some strains of bacteria to the action of cement mortars. The study revealed that, after 24 h of incubation, the planktonic growth of the *E. coli* strain is significantly inhibited in the presence of cement mortar MZH, compared to the control strain. An inhibitory activity was

observed for cement mortar MZH on *S. aureus*, *P. aeruginosa*, and *S. enterica*. Plain cement mortar E has the best growth inhibitory activity for *E. coli*. In all tests, the MZH cement mortar (with zinc oxide/hydroxyapatite powder inside) inhibited the growth of bacterial strains more than the plain cement mortar E.

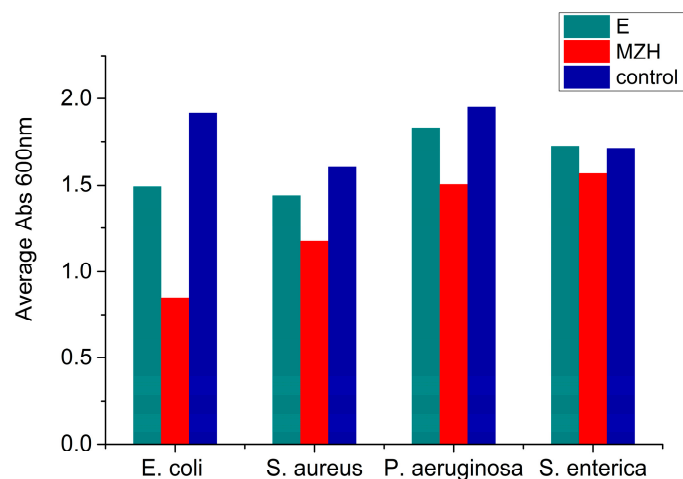


Figure 6. Demonstration of the sensitivity of some strains of bacteria to the action of cement mortars on the TSA medium: Escherichia coli ATCC 25922 (*E. coli*); Salmonella enterica ATCC 14028 (*S. enterica*); Pseudomonas aeruginosa ATCC 15442 (*P. aeruginosa*); Staphylococcus aureus ATCC 25923 (*S. aureus*).

4. Conclusions

In this study, plain cement mortar E and MZH cement mortar with particles were prepared. The MZH cement mortars with particles were obtained using standardized composition applied in industrial production (with hardening at 28 days).

The ZH powder has uniform morphology with two types of crystals. Hydroxyapatite does not substitute zinc in the structure of zinc oxide; the two types of crystals form a compound through physical bonds due to the pressure applied in the hydrothermal synthesis. Rhodamine B and methylene blue degradation results indicate that MZH cement mortar with particles exhibits better performance. In all antibacterial tests, the cement mortar MZH inhibited the growth of bacterial strains more than the plain cement mortar E. Hydroxyapatite added to cement mortar has improved its antibacterial and self-cleaning properties due to its properties.

Author Contributions: Conceptualization: A.-M.M. and I.M.; methodology: A.-M.M.; formal analysis: A.-M.M., I.M., I.A.T., I.P., S.N., M.G., A.N.G., N.V., M.A.I. and M.E.; supervision: R.M.P.; writing—original draft preparation, A.-M.M.; writing—review and editing, A.-M.M. All authors have read and agreed to the published version of the manuscript.

Funding: The work was supported by a grant of the Romanian Ministry of Research, Innovation and Digitalization, CCCDI-UEFISCDI, project number PN-III-P2-2.1-PED-2019-4829, within PNCDI III.

Data Availability Statement: Not applicable.

Conflicts of Interest: The authors declare no conflict of interest.

References

- Geng, Z.; Xin, M.; Zhu, X.; Xu, H.; Cheng, X.; Wang, D. A review: A new method for preparing photocatalytic cement-based materials and the investigation on properties and mechanism. *J. Build. Eng.* **2021**, *35*, 102080. [[CrossRef](#)]
- Guo, M.Z.; Maury-Ramirez, A.; Chi, S.P. Photocatalytic activities of titanium dioxide incorporated architectural mortars: Effects of weathering and activation light. *Build Environ.* **2015**, *94*, 395–402. [[CrossRef](#)]
- Goffredo, G.B.; Accoroni, S.; Totti, C. Titanium dioxide-based nano-treatments to inhibit microalgal fouling on building stone surfaces. *Build Environ.* **2017**, *112*, 209–222. [[CrossRef](#)]

4. Folli, A.; Pade, C.; Hansen, T.B. TiO₂ photocatalysis in cementitious systems: Insights into self-cleaning and depollution chemistry. *Cem. Concr. Res.* **2012**, *42*, 539–548. [[CrossRef](#)]
5. Mejía-de Gutiérrez, R.; Villaquirán-Caicedo, M.; Ramírez-Benavides, S.; Astudillo, M.; Mejía, D. Evaluation of the antibacterial activity of a geopolymer mortar based on metakaolin supplemented with TiO₂ and CuO particles using glass waste as fine aggregate. *Coatings* **2020**, *10*, 157. [[CrossRef](#)]
6. Wu, Y.; Lu, B.; Bai, T.; Wang, H.; Du, F.; Zhang, Y.; Cai, L.; Jiang, C.; Wang, W. Review. Geopolymer, green alkali activated cementitious material: Synthesis, applications and challenges. *Constr. Build. Mater.* **2019**, *224*, 930–949. [[CrossRef](#)]
7. Mondragón-Figueroa, M.; Guzmán-Carrillo, H.; Rico, M.A.; Reytez-Araiza, J.L.; Pineda-Piñón, J.; López-Naranjo, E.J.; Columba-Palomares, M.C.; López-Romero, J.M.; Gasca-Tirado, J.R.; Manzano-Ramírez, A. Development of a construction material for indoor and outdoor, metakaolinite-based geopolymer, with environmental properties. *J. Mater. Sci. Eng. A* **2019**, *9*, 131–142. [[CrossRef](#)]
8. Oltulu, M.; Şahin, R. Effect of nano-SiO₂, nano-Al₂O₃ and nano-Fe₂O₃ powders on compressive strengths and capillary water absorption of cement mortar containing fly ash: A comparative study. *Energ. Build.* **2013**, *58*, 292–301. [[CrossRef](#)]
9. Kumar, M.; Bansal, M.; Garg, R. An overview of beneficiary aspects of zinc oxide nanoparticles on performance of cement composites. *Mater. Today Proc.* **2021**, *43*, 892–898. [[CrossRef](#)]
10. Voicu, G.; Tiuca, G.A.; Badanoiu, A.I.; Holban, A.M. Nano and mesoscopic SiO₂ and ZnO powders to modulate hydration, hardening and antibacterial properties of Portland cements. *J. Build. Eng.* **2022**, *57*, 104862. [[CrossRef](#)]
11. Jo, B.W.; Kim, C.H.; Tae, C.; Park, J.B. Characteristics of cement mortar with nano-SiO₂ particles. *Constr. Build. Mater.* **2007**, *21*, 1351–1355. [[CrossRef](#)]
12. Sikora, P.; Augustyniak, A.; Cendrowski, K.; Nawrotek, P.; Mijowska, E. Antimicrobial activity of Al₂O₃, CuO, Fe₃O₄, and ZnO nanoparticles in scope of their further application in cement-based building materials. *Nanomaterials* **2018**, *8*, 212. [[CrossRef](#)]
13. Klapiszewska, I.; Parus, A.; Ławniczak, Ł.; Jesionowski, T.; Klapiszewski, Ł.; Ślosarczyk, A. Production of antibacterial cement composites containing ZnO/lignin and ZnO–SiO₂/lignin hybrid ad mixtures. *Cem. Concr. Compos.* **2021**, *124*, 104250. [[CrossRef](#)]
14. Cai, Y.; Hou, P.; Cheng, X.; Du, P.; Ye, Z. The effects of nano-SiO₂ on the properties of fresh and hardened cement-based materials through its dispersion with silica fume. *Constr. Build. Mater.* **2017**, *148*, 770–780. [[CrossRef](#)]
15. Kontoleontos, F.; Tsakiridis, P.E.; Marinos, A.; Kaloidas, V.; Katsioti, M. Influence of colloidal nanosilica on ultrafine cement hydration: Physicochemical and microstructural characterization. *Constr. Build. Mater.* **2012**, *35*, 347–360. [[CrossRef](#)]
16. Nath, D.; Jangid, K.; Susaniya, A.; Kumar, R.; Vaish, R. Eggshell derived CaO-Portland cement antibacterial composites. *Compos. C* **2021**, *5*, 100123. [[CrossRef](#)]
17. Adnan, M.A.M.; Julkapli, N.M.; Amir, M.N.I.; Maamor, A. Effect on different TiO₂ photocatalyst supports on photo-decolorization of synthetic dyes: A review. *Int. J. Environ. Sci. Tehnol.* **2019**, *16*, 547–566. [[CrossRef](#)]
18. Dehkordi, B.A.; Nilforoushan, M.R.; Talebian, N.; Tayebi, M. A comparative study on the self-cleaning behavior and antibacterial activity of Portland cement by addition of TiO₂ and ZnO nanoparticles. *Mater. Res. Express* **2021**, *8*, 035403. [[CrossRef](#)]
19. Esmaili, M.; Nilforoushana, M.R.; Tayebi, M.; Aghaie, E. Effect of micro/nano TiO₂ addition on the densification behavior and mechanical properties of multifunctional resistant porcelains. *Ceram. Int.* **2021**, *47*, 17435–17444. [[CrossRef](#)]
20. Mohammadi, H.; Nilforoushan, M.R.; Tayebi, M. Effect of nanosilica addition on bioactivity and in vivo properties of calcium aluminate cement. *Ceram. Int.* **2020**, *46*, 4335–4343. [[CrossRef](#)]
21. Rossi, M.; Ghiara, M.R.; Chita, G.; Capitelli, F. Crystal-chemical and structural characterization of fluorapatites in ejecta from Somma-Vesuvius volcanic complex. *Am. Mineral.* **2011**, *96*, 1828–1837. [[CrossRef](#)]
22. Baldassarre, F.; Altomare, A.; Corriero, N.; Mesto, E.; Lacalamita, M.; Bruno, G.; Sacchetti, A.; Dida, B.; Karaj, D.; Ventura, G.D.; et al. Crystal Chemistry and Luminescence Properties of Eu-Doped Polycrystalline Hydroxyapatite Synthesized by Chemical Precipitation at Room Temperature. *Crystals* **2020**, *10*, 250. [[CrossRef](#)]
23. Stern, Y.; Barulli, D. Cognitive reserve. *Handb. Clin. Neurol.* **2019**, *167*, 181–190. [[CrossRef](#)] [[PubMed](#)]
24. Muşat, V.; Anghel, E.M.; Zaharia, A.; Atkinson, I.; Mocioiu, O.C.; Buşilă, M.; Alexandru, P. A Chitosan–Agarose Polysaccharide-Based Hydrogel for Biomimetic Remineralization of Dental Enamel. *Biomolecules* **2021**, *11*, 1137. [[CrossRef](#)]
25. Dorozhkin, S.V. Functionalized calcium orthophosphates (CaPO₄) and their biomedical applications. *J. Mater. Chem. B* **2019**, *7*, 7471. [[CrossRef](#)]
26. SR EN 998-1:2016; Specification for Mortar for Masonry—Part 1: Rendering and Plastering Mortar. European Standard (EN) translated in Romanian (SR) by Romanian Standards Association (ASRO): Bucuresti, Romania, 2016.
27. SR EN 1015-11:2020; Methods of Test for Mortar for Masonry—Part 11: Determination of Flexural and Compressive Strength of Hardened Mortar. European Standard (EN) translated in Romanian (SR) by Romanian Standards Association (ASRO): Bucuresti, Romania, 2020.